SLAC–PUB–5072
October 1989
(I)

THE FAST SIMULATION OF ELECTROMAGNETIC AND HADRONIC SHOWERS*

G. Grindhammer,[a,b] M. Rudowicz,[b] and S. Peters[b]

[a] *Stanford* Linear Accelerator Center, Stanford University, Stanford, CA 94309

[b] *Max-Planck*-Institut *für* Physik und Astrophysik,
Werner-Heisenberg-Institut *für* Physik, O-8000 Miinchen 40

Presented ***by G.*** Grindhammer

Abstract

A program for the fast simulation of electromagnetic and hadronic showers using parameterizations for the longitudinal and lateral profile is described. The fluctuations and correlations of the parameters are taken into account in a consistent way. Comparisons with data over a wide energy range are made.

Invited talk presented at the SSC Workshop on Calorimetry for the Superconducting Super Collider, Tuscaloosa, Alabama, March 13-17, 1989, and Submitted to Nuclear Instruments and Methods.

* Work supported by Department of Energy contract DE–AC03–76SF00515.

1. Introduction

Particle showers in calorimeters and particularly in sampling calorimeters are typically simulated by tracking all secondary particles of the shower down to some minimum energy. The computer time needed for simulations of this type increases linearly with the shower energy and can easily become prohibitive. The parameterization of the energy density distribution of showers has been one method to speed up the simulation.

A simple algorithm for parameterized showers has been successfully used for the simulation of the UA1 calorimeter [1]. The simulation of the longitudinal energy profile of electromagnetic showers was based on fitting the parameters of an ansatz by Longo and Sestili [2] to the mean shower profile. Later, the parameterized simulation was much improved when the shape fluctuations of individual showers were systematically taken into account [3, 4]. We have extended the sophistication reached in the parameterized simulation of electromagnetic showers to hadronic showers by taking into account their individual fluctuations and, in particular, the fluctuation of their π^0 component.

This is of importance for a correct simulation of the ***e/h*** response and the energy resolution of a calorimeter, which is of great importance for the experiments being set up at the ***ep*** collider HERA and at other currently operating or planned high energy colliders.

The program GFLASH, which we have developed, generates electromagnetic and hadronic showers and computes the visible energy fraction in a geometry defined by the user with the help of GEANT [5]. In addition, GEANT is used for the tracking of particles and the accompanying physics processes, at least until the first inelastic interaction.

2. Procedure

To arrive at a useful ansatz for the longitudinal and lateral energy profiles, and to obtain the necessary parameters, we used the following iterative procedure [6]:

- use/modify an ansatz and fit the parameters to Monte Carlo (MC) data using a detailed simulation of electromagnetic and hadronic showers[5,7]; and
- compare and fit some of the parameters with experimental data.[8]

The MC data were generated for the typical sampling structures of the H1 calorimeter[8,9] built for the H1 experiment at HERA. The essential materials of this calorimeter are lead (Pb) and liquid argon (LAr) for the electromagnetic and iron (Fe) and LAr for the hadronic modules. Showers in the energy range from 1 to 200 GeV were generated. The parameters, and their fluctuations and correlations, were parameterized as a function of energy, using scales which minimize the dependence on the calorimeter materials.

The simulation of showers in GFLASH has been divided into two steps. First, the spatial distribution of the deposited energy E_{dp} for a shower is calculated for the calorimeter module containing all or part of the shower, taking the fluctuations and correlations of the parameters and their energy dependence into account:

$$dE_{dp}(\vec{r}) = E_{dp}\, f(z)\, dz\, f(r)\, dr\, f(\phi)\, dr\, \phi \,. \qquad (1)$$

A calorimeter module or a part of it-which may have a complicated, but repetitive, sampling structure-is described by one single effective medium. In the second step, the energy fraction of the deposited energy which is visible in the active medium E_{vs} is computed

$$dE_{vs}(\vec{r}) = E_{dp}\, \widetilde{mip} \sum_k \frac{\tilde{k}}{\widetilde{mip}}\, c_k\, f_k(\vec{r})\, dV \,. \qquad (2)$$

Here, $\widetilde{mip}$ denotes the sampling fraction for minimum ionizing particles, and $\tilde{e}/\widetilde{mip}$ and $had/\widetilde{mip}$ are the relative sampling fractions for electrons and hadrons, respectively. The sum is over the electromagnetic (k = e) and the purely hadronic (k = had) components, taking the distribution functions f_k for the two components and their relative fractions c_k of the energy deposited in the active medium into account. For the calorimeter-dependent sampling fractions $\widetilde{mip}$, $\tilde{e}$, $\widetilde{had}$, and the sampling fluctuations, it is desirable to use measured values.

3. Parameterization of electromagnetic showers

3.1. Longitudinal shower profile

It is well known that the mean longitudinal profile of electromagnetic showers can be described by a Gamma distribution [2]. A realistic simulation, however, requires the simulation of individual showers. Fluctuating the parameters obtained from average profiles does not necessarily lead to a correct description of the fluctuations of individual showers [4]. Assuming that the individual shower profiles can also be approximated by a Gamma distribution

$$f_i(z) = \frac{x^{\alpha_i - 1}\, e^{-x}}{\Gamma(\alpha_i)} \quad , \qquad \text{with} \qquad x = \beta_i z \quad , \tag{3}$$

the fluctuations can be deduced and reproduced. The index i indicates that the function describes an individual shower i with the parameters α_i and β_i. The shower depth z is measured in units of radiation length $[X_0]$. The α_i and β_i can be calculated from the first and second moments of the Gamma distribution. They are normal-distributed such that the means μ_α and μ_β, and their fluctuations σ_α and σ_β can be determined and parameterized as a function of energy. The correlation of the α_i and β_i is given by

$$\rho = \frac{\langle (\alpha_i - \langle \alpha_i \rangle)\,(\beta_i - \langle \beta_i \rangle) \rangle}{\left[\left(\langle \alpha_i^2 \rangle - \langle \alpha_i \rangle^2 \right) \left(\langle \beta_i^2 \rangle - \langle \beta_i \rangle^2 \right) \right]^{1/2}} \quad . \tag{4}$$

Numerically, $\rho = 0.73$ and is roughly independent of the energy of the shower in the range from 1 to 200 GeV. In the simulation, a correlated pair (α_i, β_i) is generated according to

$$\begin{pmatrix} \alpha_i \\ \beta_i \end{pmatrix} = \begin{pmatrix} \mu_\alpha \\ \mu_\beta \end{pmatrix} + C \begin{pmatrix} z_1 \\ z_2 \end{pmatrix} \quad , \qquad \text{with}$$
$$C = \begin{pmatrix} \sigma_\alpha & 0 \\ 0 & \sigma_\beta \end{pmatrix} \begin{pmatrix} \sqrt{(1+\rho)/2} & \sqrt{(1-\rho)/2} \\ \sqrt{(1+\rho)/2} & -\sqrt{(1-\rho)/2} \end{pmatrix} \quad , \tag{5}$$

where z_1 and z_2 are normal-distributed random numbers.

The whole procedure is presented graphically in fig. 1 for 10 GeV e^- showers. The individual and the mean energy profiles of 400 showers, as generated with GEANT and with GFLASH, are shown. In addition, the distribution of the parameters α_i and β_i, and their correlation as obtained from GEANT, are given. A comparison of the GEANT and GFLASH simulation reveals good agreement in the mean profiles (additional energies are compared in fig. 2) and in the individual fluctuations, particularly in the variation of the center of gravity and the shower maximum.

3.2 *Lateral shower profile*

For the description of the lateral energy profile of electromagnetic as well as hadronic showers, we assume only a radial, and no azimuthal dependence. The average radial shower distribution is frequently described by the superposition of two exponentials (see e.g., ref. 10). One of them describes the confined energetic core of the shower and the other the surrounding halo.

In GFLASH, we have used the very simple ansatz

$$f(r) = \frac{2\, r\, R_{50}^2}{(r^2 + R_{50}^2)^2} , \qquad (6)$$

for both electromagnetic and hadronic showers, which seems quite adequate, at least as long as the lateral resolution of the calorimeter is of the order of or larger than $\sim$ 1 Moliere radius (R_M) for electromagnetic and $\sim$ 0.1 absorption length (λ_0) for hadronic showers. The radius r and the free parameter R_{50} in eq. (6) are in units of R_M (or λ_0 for hadronic showers). Fixed amounts of energy (energy spots) are deposited at radii r, generated according to the radial probability function. To simulate the fluctuations of individual showers, it is necessary to parameterize the mean and the variance ***(V)*** of the approximately log-normal distributed parameter R_{50} as a function of shower energy ***E*** [GeV] and shower depth z [in units of X_0 or λ_0]:

$$\begin{aligned} \langle R_{50}(E,z)\rangle &= [R_1 + (R_2 - R_3 \ln E)\, z]^n , \\ V_{R_{50}}(E,z) &= [(S_1 - S_2 \ln E)\, (S_3 + S_4\, z)\, \langle R_{50}(E,z)\rangle]^2 . \end{aligned} \qquad (7)$$

This parameterization, with n = 1 (2) for hadronic (electromagnetic) showers,

describes the increasingly slower growth of the radial extent and of the relative fluctuations $\sqrt{V_{R_{50}}}/\langle R_{50}\rangle$ of a shower with increasing energy. Lateral distributions for 10 GeV e^- showers as a function of depth generated with GEANT and GFLASH are compared in fig. 3. As can be seen, there is reasonable agreement in the description of the hard core and halo of the showers.

3.3. Sampling fluctuations

The conversion from the deposited energy to the fraction which is visible in the active part of the sampling structure is performed during the lateral depositioning of the energy spots. In addition, the sampling fluctuations are taken into account.

The visible energy for a spot is computed using the measured sampling fractions $\widetilde{mip}$ and the relative fraction $\tilde{e}/\widetilde{mip}$ (and, in addition, $\widetilde{had}/\widetilde{mip}$ for hadron showers), which may depend on the position of the spot in the calorimeter. The sampling fluctuations are reproduced by depositing a Poisson distributed number of spots $N_s(\ell)$ of energy E_s per longitudinal integration interval ℓ according to the radial probability function. Assuming the energy resolution to be simulated is given by

$$\frac{\sigma_{dp}}{E_{dp}} = \frac{a}{\sqrt{E_{inc}}} \quad , \qquad \text{and with}$$

$$\sigma_{dp}^2 = V\left[\sum_{\ell} E_s\, N_s(\ell)\right] = E_s^2 \sum_{\ell} V\left[N_s(\ell)\right] = E_s\, E_{dp} \quad , \tag{8}$$

we find for the spot energy:

$$E_s = a^2 \quad .$$

4. Parameterization of hadronic showers

It is convenient to imagine a hadronic shower as consisting of a purely hadronic and a π^0 component (mainly π^0's and some η's). The large fluctuations of the relative fractions of the π^0 and hadronic components in a shower lead to

fluctuations in a noncompensating calorimeter (e/h $\neq 1$), which are much larger than the fluctuations of electromagnetic showers alone. A simulation of hadronic showers has to take into account:

- the energy dependence of the fraction of the π^0 component (c_{π^0}) and its fluctuation;
- the response of the calorimeter which, in general, differs for the π^0 and the purely hadronic showers; and
- the different propagation scales, X_0 for the π^0 and λ_0 for the hadronic component.

*4.1. **Longitudinal parameterisation***

A well-known ansatz for the parameterization of the mean longitudinal energy profile [1] uses the superposition of two Gamma distributions to describe the π^0 and the purely hadronic subprofiles:

$$dE_{dp} = E_{dp}\,[(1 - c_{\pi^0})\,\mathcal{H}(x)\,dx + c_{\pi^0}\,\mathcal{E}(y)\,dy] \quad , \tag{9}$$

$$\text{with} \qquad \mathcal{H}(x) = \frac{x^{\alpha_h - 1}\, e^{-x}}{\Gamma(\alpha_h)} \quad , \qquad \text{and} \qquad x = \beta_h\, s_h \quad ,$$

$$\text{with} \qquad \mathcal{E}(y) = \frac{y^{\alpha_e - 1}\, e^{-y}}{\Gamma(\alpha_e)} \quad , \qquad \text{and} \qquad y = \beta_e\, s_e \quad .$$

The distance from the shower starting point is given by s_h [λ_0] for the hadronic and by s_e [X_0] for the π^0 component.

We used this ansatz to describe the mean shower energy profile obtained from a simulation of the H1 calorimeter, using GEANT. A satisfactory description of the shower shapes could only be obtained if one allowed the parameter c_{π^0} to decrease with energy which is inconsistent with data [8]. This behavior has also been observed by fitting data with a similar method [11,12]. It is, however, necessary to correctly simulate the π^0 and hadronic subprofiles individually in order to compute their different responses and the fluctuations of individual showers properly. We expected an ansatz containing three terms to accomplish this:

$$dE_{dp} = f_{dp}\, E_{inc} \left[c_h\, \mathcal{H}(x)\, dx + c_f\, \mathcal{F}(y)\, dy + c_l\, \mathcal{L}(z)\, dz \right] , \tag{10}$$

with $\mathcal{H}(x) = \frac{x^{\alpha_h - 1}\, e^{-x}}{\Gamma(\alpha_h)}$, and $x = \beta_h \left[\lambda_0^{-1}\right] s_h \left[\lambda_0\right]$;

with $\mathcal{F}(y) = \frac{y^{\alpha_f - 1}\, e^{-y}}{\Gamma(\alpha_f)}$, and $y = \beta_f \left[X_0^{-1}\right] s_f \left[X_0\right]$;

with $\mathcal{L}(z) = \frac{z^{\alpha_l - 1}\, e^{-z}}{\Gamma(\alpha_l)}$, and $z = \beta_l \left[\lambda_0^{-1}\right] s_l \left[\lambda_0\right]$.

As before, the first term describes the purely hadronic shower profile. The second term models the subprofile of the π^0 fraction which is produced in the first inelastic interaction(the index f stands for "first"). Its scale is measured in X_0. The third term simulates the subprofile of the π^0 fraction, which is produced in the course of the further development of the shower (the index ℓ stands for "late"). It scales in λ_0. The fraction of deposited energy (f_{dp}) with respect to the energy of the incident particle (E_{inc}) takes the intrinsic losses during the hadronic shower development into account.

Assuming an energy dependence of the form $a + b \ln E$ for the parameters to be fitted, a good description of the mean energy profile was achieved. This can be seen in fig. 4, which shows the results of the fits to the mean shower profiles for different energies simulated with GEANT. However, despite this good agreement, two problems remained. One problem was that one needed two sets of parameters, one for $1 \lesssim E_{inc} \lesssim 5$ and one for $5 < E_{inc}\,[\mathrm{GeV}] \lesssim 200$, and the other problem was that for some of the parameters a normal or log-normal distribution was not a good approximation. Both of these "defects" could be remedied by taking the relative probabilities for the occurrence of the different subprofiles into account.

4.2. π^0 fluctuations

To simulate the π^0 fluctuations, it is not sufficient to just fluctuate the average fractions c_h, c_f, and c_ℓ of the deposited energy [see eq. (lo)]. The reasons are:

- not every hadronic shower with energy $\lesssim 5$ GeV yields a π^0 in the first inelastic interaction; and
- up to an energy of about 50 GeV, also no "late" π^0 may be produced.

In fig. 5, the relative probabilities for a hadronic shower to have any π^0's $P(\pi^0)$, to have a π_f^0 and a π_ℓ^0 component $P(\pi_f^0$ and $\pi_\ell^0)$, and to have only a π_ℓ^0 fraction $P(\pi_\ell^0)$ are shown as simulated by GEANT. We distinguish three classes of hadronic showers according to our ansatz:

1) purely hadronic showers:

   class ***H*** with $P(\pi^0) < P \leq 1$,

2) showers containing a π_f^0 component:

   class F with $P(\pi_f^0$ and $\pi_\ell^0) < P \leq P(\pi^0)$, and

3) showers which in addition to π_f^0 also contain a π_ℓ^0 component:

   class ***L*** with $0 < P \leq P(\pi_f^0$ and $\pi_\ell^0)$,

   where P is a uniform distributed random number.

Taking these probabilities into account and distinguishing between the three shower classes finally allows us to successfully simulate individual hadronic showers using eq. (10). The fractions c_h , c_f , and c_l are calculated according to:

$$\begin{aligned} c_h\ (E) &= 1 - f_{\pi^0}\ (E) \\ c_f\ (E) &= f_{\pi^0}\ (E)\ (1 - f^l_{\pi^0}\ (E)) \\ c_l\ (E) &= f_{\pi^0}\ (E)\ f^l_{\pi^0}\ (E) \end{aligned} \tag{11}$$

$$\text{with} \quad c_h(E) + c_f(E) + c_l(E) = 1 \ ,$$

$$\text{and} \quad f_{\pi^0} = \left\langle \frac{E_{\pi^0}}{E_{dp}} \right\rangle \ , \quad f^l_{\pi^0} = \left\langle \frac{E^l_{\pi^0}}{E_{\pi^0}} \right\rangle \ .$$

The energy dependence of the mean π^0 fractions as obtained from GEANT are shown in fig. 6. The fractional π^0 energy of an individual shower is then given by $f_{\pi^0}/P(\pi^0)$, which is also displayed in fig. 6.

As in the case of electromagnetic showers, individual shower profiles are used to obtain the means, fluctuations and correlations of the parameters f_{dp} , f_{π^0} , $f^l_{\pi^0}$,

α_h , β_h , α_f , β_f , α_l , and β_l . For shower class ***H,*** there are three; for class F, there are six; and for class ***L,*** there are nine parameters whose means and covariances are parameterized as a function of energy.

The vector of parameters $\vec{x}$ for an individual shower is given by [13]

$$\vec{x} = \vec{\mu} + C\vec{z} \quad , \qquad \text{with} \qquad V = CC^T \quad . \tag{12}$$

The vector $\vec{z}$ contains maximally nine normal-distributed random numbers with variance of one, $\vec{\mu}$ is the vector of the means of the parameters and ***V*** is their covariance matrix. A method by Cholesky [14] is used to decompose the n-dimensional symmetric matrix ***V.*** To use the more intuitive parameters σ_{ii} and ρ_{ij} instead of the covariance V_{ij} , it is the correlation matrix ρ which is decomposed in GFLASH after the transformation $\boldsymbol{V} = \sigma\rho\sigma^T$ with the diagonal matrix σ.

For the simulation of the lateral shower distribution and the sampling fluctuations, the same functional form and basically the same method are used as for electromagnetic showers.

5. The GEANT–GFLASH interface

The interfacing of GFLASH with GEANT was done for the following reasons:

- Like many other experiments, the H1 collaboration has decided to use GEANT for the description of the detector geometry in its simulation program. With GFLASH implemented in GEANT, it is then very easy for the user to switch between simulations of showers using GEANT/GHEISHA [5,7] or the parameterization algorithm of GFLASH. In addition, in this scheme, GEANT can be used for the first inelastic interaction(s) (for example, until the energies of the secondaries of a very high energy incident particle have cascaded down to the energy range for which the parameterization in GFLASH has been tested), switching to GFLASH for the remaining secondaries.
- When using GFLASH, it is appropriate to describe a calorimeter module of the same type with one medium characterized by a suitable average over the properties of the materials of that module. This considerably reduces the time spent by GEANT in searching for volumes and tracking.

- The major part of the energy of a shower is deposited inside a small cylinder of about one R_M for electromagnetic showers, and less than an λ_0 for hadronic showers. To a good approximation, therefore, the shower development is determined by the medium found at the core of the shower. The "tracking" routines of GEANT are used to provide GFLASH with the geometry and material information it needs.

In fig. 7, we show a simplified schematic of GEANT and the integration of the relevant GFLASH routines (underlined). A trivial change in GTVOL permits attachment of GFLASH.

The routine GTREVE administers the tracking of the primary tracks of the event (prim-tracks) and of the secondary tracks (sec_tracks) generated during tracking by various physics processes. GTRAK, using geometry information (geombanks), tracks particles through the different volumes. Within a given volume, it is the task of GTVOL to call the particle-type specific routines for the simulation of physical processes. These are the routines GTGAMA for photons, GTELEC for e^+ and e^-, GTNEUT for neutrons, GTHADR for all other hadrons, GTMUON for μ's, and GTNINO for ν's. The- energy loss DESTEP' calculated in these routines and the generated secondary particles [GKIN (5,NGKINE)] are passed on to the user routine GUSTEP. At this point, GFLASH can be attached. If an inelastic reaction has taken place in a volume belonging to the calorimeter, then this point is taken to be the starting point for the shower development. Whether the ensuing shower development will be parameterized or continued to be simulated in detail can be made dependent on boundary conditions determined by the user. If the shower is to be generated by GFLASH, a "pseudoshower-particle" with the four-momentum of the incident particle (the energy is modified, depending on the incident particle type), initiating the inelastic reaction is created and stored (sec_tracks). The tracking of the original particle is stopped. Standard GEANT routines can be used to track the "pseudoshower-particle" through the detector and to get the material parameters (X_0, λ_0, A, Z, and R_M) necessary for the generation of the longitudinal and lateral shower profiles. This is accomplished by inserting one call to the GFLASH routine GTEMSH (for electromagnetic shower simulation) and one to GTHASH (for hadronic shower simulation)

into the GEANT routine GTVOL. This small change in GTVOL is the only change needed inside a GEANT routine.

After generating the longitudinal energy profile for a shower in GTEMSH or GTHASH, it is integrated in small steps up to the volume boundary. For every integration step energy spots are computed according to the fluctuated lateral distribution for this step and the sampling fluctuations for the volume the spot is in. The visible fraction of the deposited energy of a spot is calculated in GFSPOT after mapping the spot coordinates to read out channel numbers of the calorimeter. The same routine as for the detailed simulation is used for the mapping of the approximately 40000 channels of, the H1 calorimeter. Nonsensitive regions of the calorimeter are simulated through the mapping of the energy spots onto those regions. Finally, the visible energy and channel number are stored for digitization (cal_hit_banks in fig. 7).

6. Comparison with data

We compared GFLASH with data from the H1 calorimeter test [8] at CERN using hadron beams. The comparisons shown were made after some of the parameters of GFLASH had been tuned using this data. The longitudinal segmentation of the test calorimeter is shown schematically in fig. 8. The beam enters the EC module (Pb/LAr, 1.13 λ_0, four segments) from the right. Next, the HC (Fe/LAr, 3.76 λ_0, four segments) and the "tail catcher" TC (Fe/LAr, 2.88 λ_0, two segments) with thicker iron plates follow. Superimposed on the drawings are a graphic representation of a 30 GeV π^- shower simulated by GEANT [fig. 8(a)] and the energy spots of GFLASH [fig. 8(b)].

6.1. Longitudinal and lateral profiles

The mean longitudinal energy profile for hadronic showers from the experiment and the profile as simulated by GFLASH for different energies are shown in fig. 9 (in linear and log scale) and fig. 10. In addition, the profiles as predicted by GEANT (with GHEISHA7) and by GHEISHA8 [ref. 8] are presented in fig. 9. The excellent agreement of GFLASH with the experimental profile is a consequence of

the refitting of some of the GFLASH parameters. Figure 10 shows the development of a second maximum in the segment HC_2 with increasing energy which is well-simulated by GFLASH. This effect can be understood as follows. The lengths (in λ_0) of EC_4, HC_1, and HC_2 increase such that roughly equal numbers of showers are starting in these segments. However, in units of X_0, due to the difference in the ratios of X_0 to λ_0 for Pb and Fe, the segment HC_1 is shorter than the neighboring segments. While an electromagnetic subshower of a few GeV starting in EC_4 or HC_2 will be almost completely contained there, such a subshower starting in HC_1 will leak some of its energy into HC_2. The correct simulation of this effect by GFLASH indicates a good parameterization of the π^0_f fraction of the shower.

The dependence of the mean lateral profile on the shower depth and energy can be seen in fig. 11 where the lateral charge distribution as a function of depth is shown for one energy, and in fig. 12 where it is plotted for different energies at a fixed depth. There is good agreement between GFLASH and the experiment for the core as well as the halo of the shower.

6.2. Fluctuations of hadronic showers

The total visible energy for the modules EC, HC, and TC (normalized to their respective sampling fractions for minimum ionizing particles) for six different beam energies is compared with the expectations from GFLASH in fig. 13. For the energy range considered, the agreement is good and the asymmetry of the distributions, which is expected for noncompensating calorimeters, is properly simulated. In this comparison of experimental and simulated data, only a single constant relating charge to energy as obtained experimentally with muons was used, and not-as is frequently done-a set of constants which is determined by demanding equality of the means with the incident energy and minimal variances.

The energy resolution of the calorimeter is shown in fig. 14 for pions as a function of energy, together with the results from the simulation. The good agreement here suggests that the intrinsic and sampling fluctuations for the Pb and Fe calorimeters are properly taken into account in GFLASH.

The visible energy seen in the three different modules (EC, HC, and TC) for 30 GeV showers is compared in fig. 15 with results from GEANT and GFLASH.

The good agreement observed for GFLASH indicates a proper handling of the different materials and sampling structures in the simulation. The pattern of slightly too much energy in EC and too little in TC, as generated by GEANT, is a consequence of the shower length of GEANT being too short, as can be noticed in fig. 9.

The first maximum seen in the visible energy in HC is due to showers starting in EC and depositing most of the π^0_f energy there, while the second maximum is due to showers originating in HC. How the visible energy distribution for the HC changes-as a function of energy and how this is simulated by GFLASH is shown in fig. 16.

The energy fluctuations and correlations for different calorimeter segments are displayed in fig. 17 for 70 GeV showers. The agreement between GFLASH and the data is quite satisfactory, even for the "long range" (EC vs. TC) correlations.

7. Speed estimate

We used the H1 detector simulation program [15], which is still under development, to provide some preliminary timing information. We took as an example 50 GeV pions which shower in the H1 forward calorimeter [9]. We found the following average times [using an IBM 3090-1503 ($\approx$ 3.5 VAX 8600)]: 85 ms for the tracking of the pion from the interaction point through the central and forward tracker volumes to the first inelastic interaction in a calorimeter volume (GEANT), 55 ms for the tracking of the "pseudoshower-particle" (GEANT), and 30 ms for the generation of the energy spots (GFLASH). This indicates that, at least in the context of H1, the time spent on the shower-specific tasks of GFLASH is small compared to the time spent on the geometry-specific tasks of GEANT. The 30 ms for GFLASH includes the time for the tracking of a shower within a volume which is done by GFLASH. Compared to a detailed simulation using GEANT/GHEISHA with standard values for the cutoff energies, we found that the simulation with GFLASH is about 180 times faster. Since neither the detailed nor the parameterized simulation, as such, were particularly optimized for speed, the numbers given above should be taken with caution.

A simulation of the H1 test calorimeter (as shown in fig. 10) by GFLASH and GEANT/GHEISHA leads to the CPU time requirements (using an IBM 3090–180E) as given in Table 1. The times given for GFLASH depend on the parameterization chosen for the number of energy spots as a function of energy, which in turn depends on the geometry and size of the readout channels. In-this example, 200 (250) spots were generated for 50 (200) GeV.

Perhaps more important in the comparison of the time required for the detailed and parameterized simulation of showers is their energy dependence. Due to theproportionality of energy and total track length of a shower, the computer time required for simulation with GEANT/GHEISHA increases linearly with energy, while for GFLASH the time is proportional to the shower length which grows only logarithmically with energy.

8. Conclusions

GFLASH[◇] provides a realistic and fast parameterization for the simulation of electromagnetic and hadronic showers in a geometry defined by the user with GEANT. The longitudinal and lateral distribution, their fluctuations and correlations, are modeled in a consistent way. For hadrons, this was made possible by a new ansatz for the longitudinal energy profile consisting of three Gamma distributions: one for the purely hadronic component of the shower, one for the π^0 fraction originating from the first inelastic interaction, and one for the π^0 fraction from later inelastic interactions. The interfacing of GFLASH with GEANT provides great flexibility and ease of use.

Acknowledgments

We are very much indebted to H. Greif for providing us with data tapes and information from the H1 calorimeter test at CERN. We also thank T. Hansl-Kozanecka and D. Groom for their careful reading of this manuscript. One of us (G. G.) would like to thank the SLAC directorate and M. Perl for the hospitality he is enjoying at SLAC.

◇ GFLASH is available for distribution; please contact one of the authors.

References

[1] R. K. Bock et al., Nucl. Instr. and Meth. 185 (1981) 533;
M. della Negra, Scripta Phys. 23 (1981) 469-479.

[2] E. Longo and I. Sestili, Nucl. Instr. and Meth. 128 (1975) 283.

[3] Y. Hayashide et al., CDF Note 287, Batavia, IL (1985).

[4] J. Badier and M. Bardadin-Otwinowska, ALEPH 87-9, EMCAL 87-1, Geneva (1987).

[5] R. Brun et al., GEANT3 User's Guide. CERN-DD/EE 84-1, Geneva (1986).

[6] M. Rudowicz, Diplomarbeit an der Universitat Hamburg; MPI-PAE/Exp. El. 200 (1989);
S. Peters, Diplomarbeit an der Universitat Hamburg; MPI-PAE/Exp. El. 202 (1989).

[7] GHEISHA7 as implemented in GEANT; see also H. C. Fesefeldt, PITHA Report 85/02, RWTH Aachen (1985).

[8] H1 Calorimeter Group (W. Braunschweig et al.), DESY 89/022 (1989).

[9] H1 Collaboration, Technical Proposal for the H1 Detector, DESY, Hamburg, 1986.

[10] G. A. Akopdjanov et al., Nucl. Instr. and Meth. 140 (1977) 441-445.

[11] E. Hughes, CERN CDHS Internal Note 4, Geneva (1986).

[12] W. J. Womersley et al., Nucl. Instr. and Meth. A267 (1988) 49, and erratum **A278** (1989) 447.

[13] F. James, Rep. Prog. Phys. 43 (1980) 1145-1189.

[14] R. Y. Rubinstein, Simulation and the Monte Carlo Method (John Wiley & Sons, New York, 1981).

[15] G. D. Patel et al., H1 Collaboration Internal Note, Hamburg (1988).

Table1. CPU time requirements (IBM 3090–180E) for the simulation of showers in the H1 test calorimeter.

	Energy	GFLASH	GEANT
π^+	50 GeV	26 ms	8s
π^+	200 GeV	31 ms	-32 s
e^-	50 GeV	10 ms	30 s
e^-	200 GeV	11 ms	110 s

Figure Captions

1. Longitudinal energy profile and parameters for 10 GeV e^- showers.
2. Mean longitudinal energy profile for e^- showers: GEANT (o) and GFLASH (- – –).
3. Lateral energy profile for 10 GeV e^- showers at different depths: GEANT (left) and GFLASH (right).
4. Mean longitudinal energy profile for π^+ showers: FIT (—) and GEANT (o).
5. Relative probabilities for different hadronic shower-classes.
6. Comparison of mean π^0 fractions for π^+-induced showers as a function of the incident energy E_{inc} : f_{π^0} is the mean π^0 fraction from all showers; $f_{\pi^0}/P(\pi^0)$ is the mean π^0 fraction from showers with a π^0 component; and $f_{\pi^0}\, f^l_{\pi^0}$ is the mean "late" π^0 fraction from all showers; GEANT (o, ❑).
7. Schematic representation of the implementation of GFLASH in GEANT.
8. Simulation of the H1 test calorimeter: (a) GEANT and (b) GFLASH.
9. Mean longitudinal energy profile for 30 GeV π^- showers: experiment (o), GFLASH (· . ·), GEANT311 (- -), and GHEISHA8 (—).
10. Mean longitudinal energy profile for π^- showers: experiment (o) and GFLASH (···).
11. Mean lateral charge profile for 30 GeV π^- showers with shower starting point in HC_1: experiment (—), GEANT (- – –), and GFLASH (· . ·).
12. Mean lateral charge profile in HC_2 for π^- showers with shower starting point in HC_1: experiment (-) and GFLASH (· . ·).
13. Energy distribution for π^- showers for beam energies 10, 30, 50 (top) and 70, 120, 170 GeV (bottom): experiment (-) and GFLASH (···).
14. Energy resolution of the calorimeter (EC + ***HC + TC)*** for π^- showers: experiment (o) and GFLASH (●).
15. Energy distributions in the modules EC, ***HC,*** and TC for 30 GeV π^- showers: experiment (—), GFLASH (· · ·), and GEANT (- – –).
16. Energy distributions for π^- showers in ***HC*** for different energies: experiment (—) and GFLASH (· . ·).
17. Energy correlations between different calorimeter modules for 70 GeV π^- showers: experiment (left) and GFLASH (right).

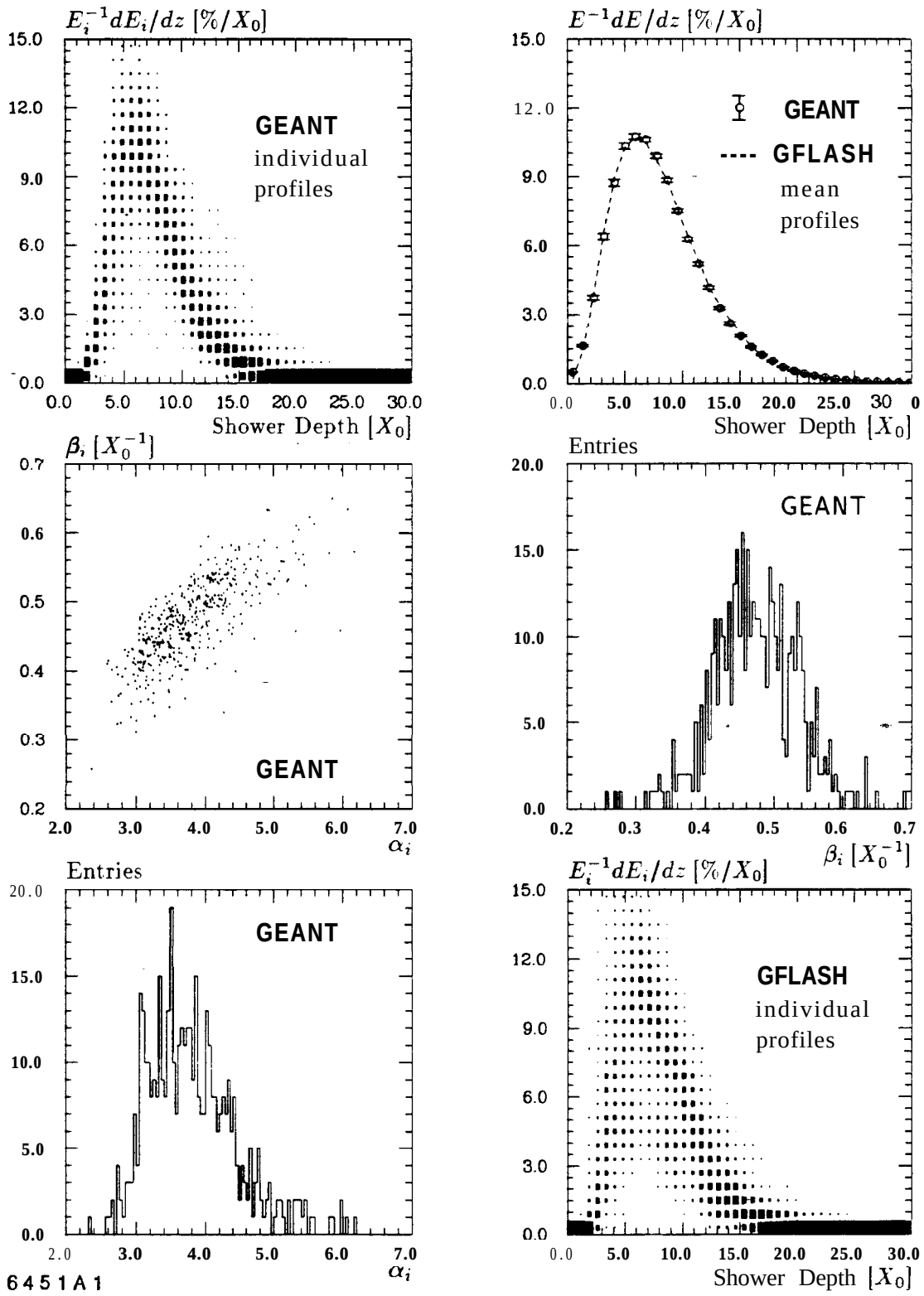
$E_i^{-1}dE_i/dz$ [%/X_0]
GEANT
individual
profiles
Shower Depth [X_0]
$E^{-1}dE/dz$ [%/X_0]
GEANT
GFLASH
mean
profiles
Shower Depth [X_0]
β_i [X_0^{-1}]
GEANT
α_i
Entries
GEANT
β_i [X_0^{-1}]
Entries
GEANT
α_i
$E_i^{-1}dE_i/dz$ [%/X_0]
GFLASH
individual
profiles
Shower Depth [X_0]
6451A1

Fig. 1

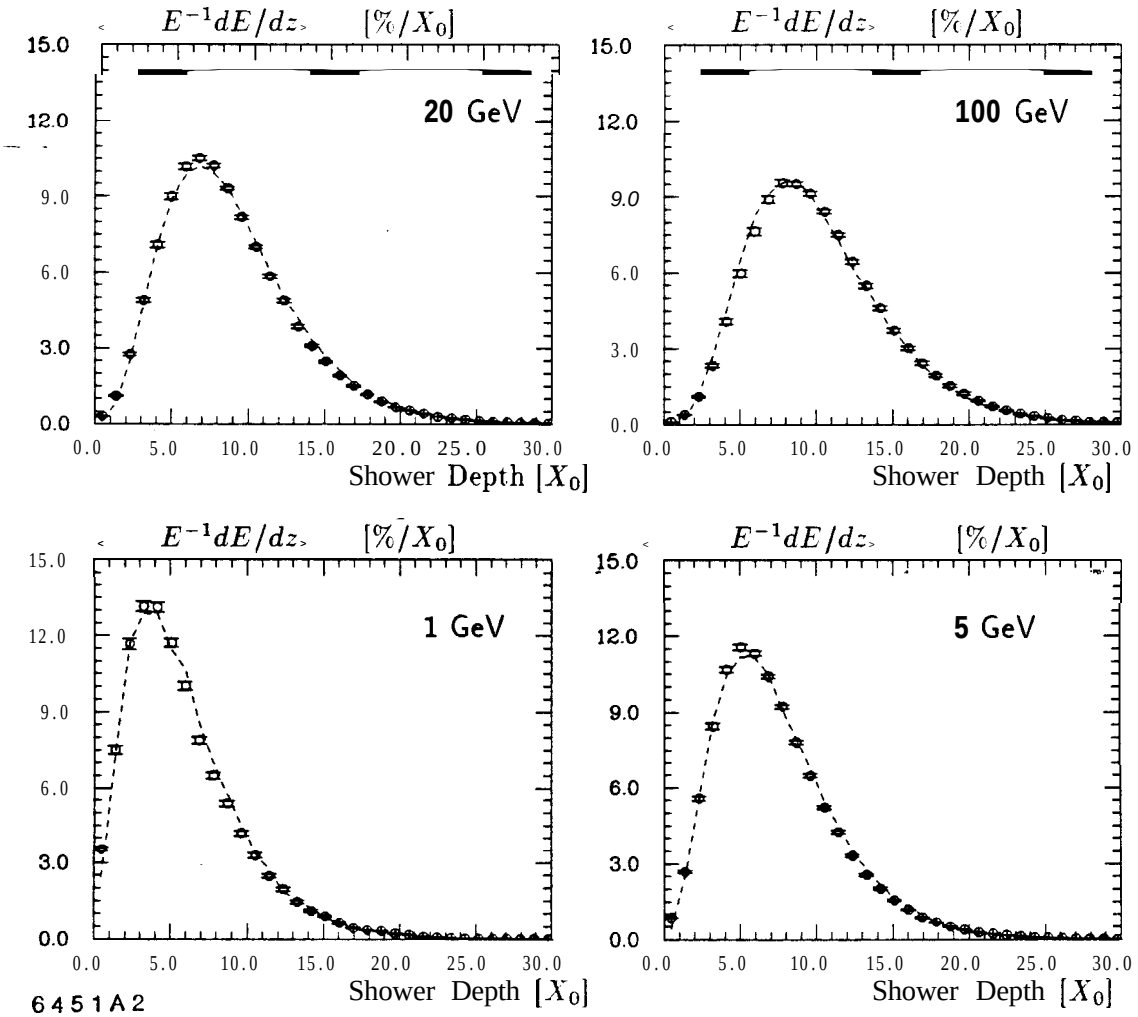
$\langle E^{-1}dE/dz \rangle$ [%/X_0]
20 GeV
100 GeV
1 GeV
5 GeV
Shower Depth [X_0]
6451A2

Fig. 2

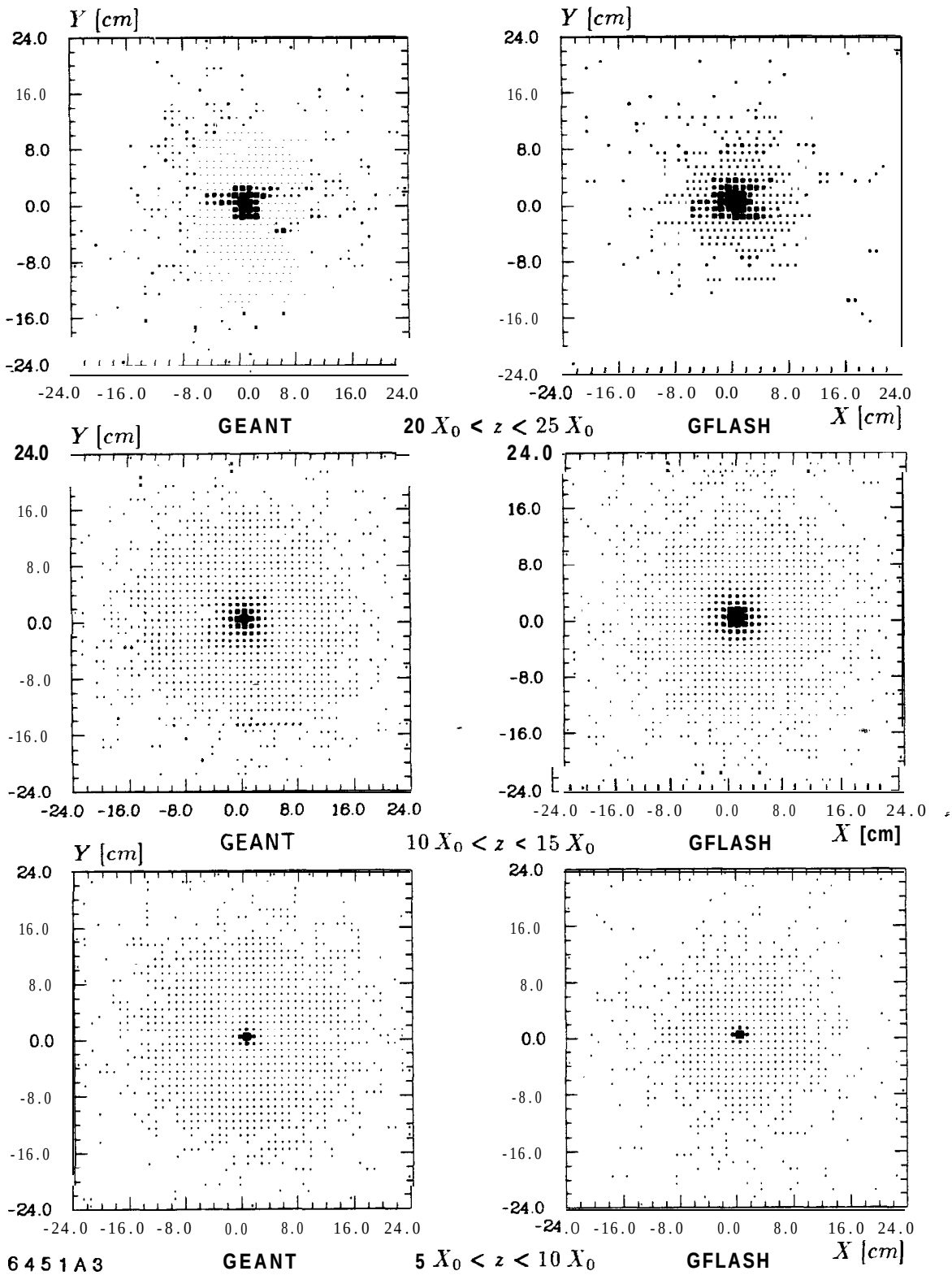
Y [cm]
24.0
16.0
8.0
0.0
-8.0
-16.0
-24.0
-24.0 -16.0 -8.0 0.0 8.0 16.0 24.0
GEANT
20 X_0 < z < 25 X_0
GFLASH
X [cm]
10 X_0 < z < 15 X_0
5 X_0 < z < 10 X_0
6451A3

Fig. 3

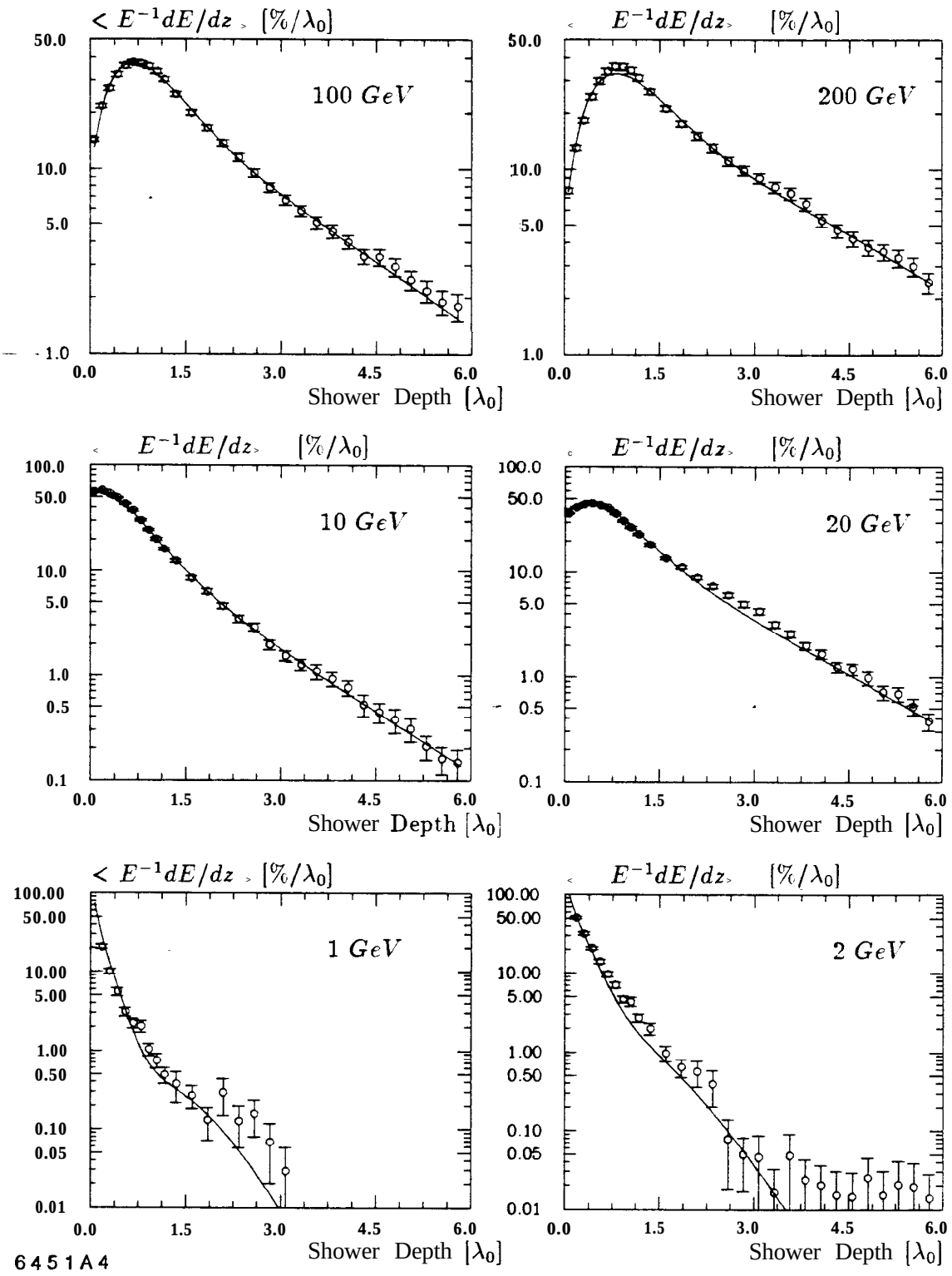
$< E^{-1}dE/dz >$ [%/λ_0]
100 GeV
200 GeV
10 GeV
20 GeV
1 GeV
2 GeV
Shower Depth [λ_0]
6451A4

Fig. 4

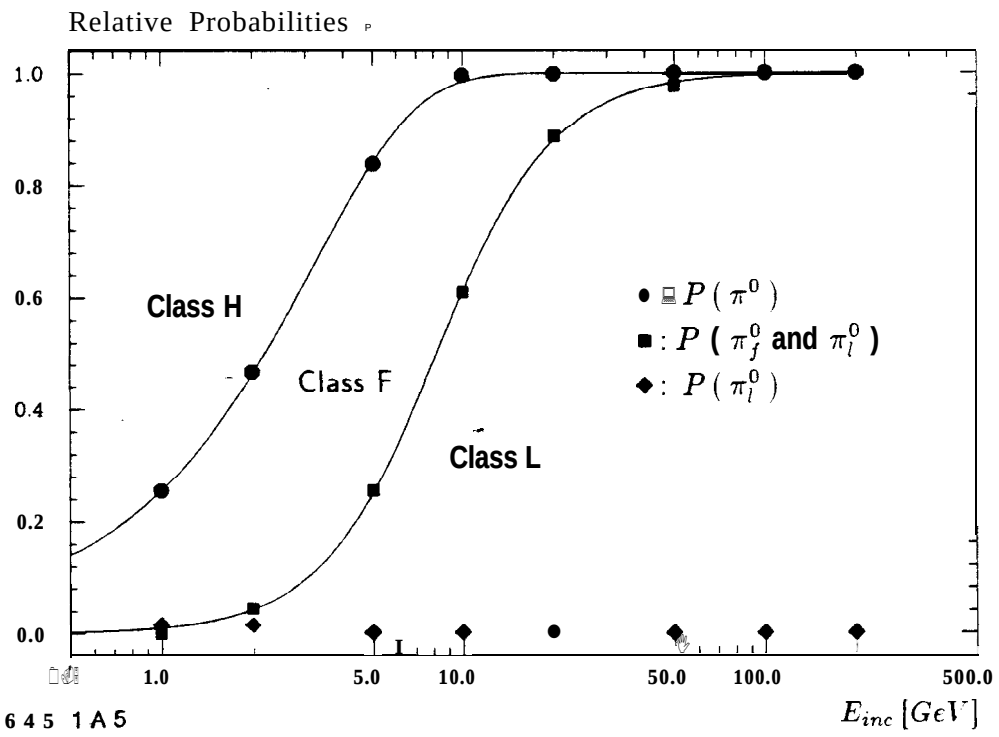
Relative Probabilities
1.0
0.8
0.6
0.4
0.2
0.0
Class H
Class F
Class L
● : $P(\pi^0)$
■ : $P(\pi_f^0$ and $\pi_l^0)$
◆ : $P(\pi_l^0)$
1.0
5.0
10.0
50.0
100.0
500.0
E_{inc} [GeV]
6 4 5 1 A 5

Fig. 5

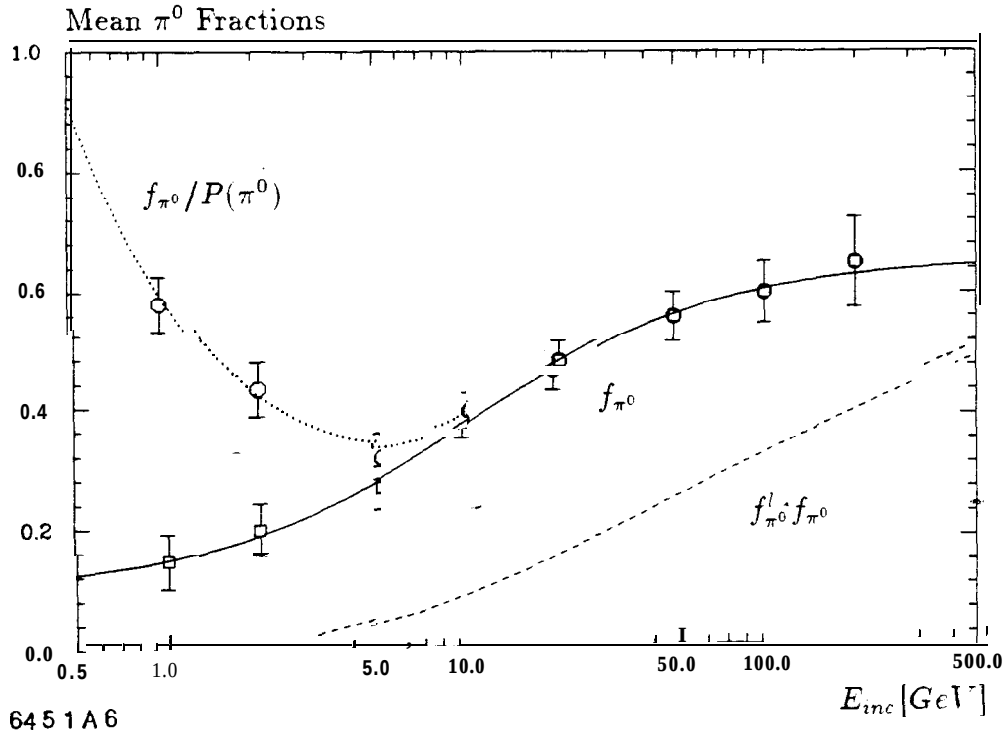
Mean π^0 Fractions
1.0
0.6
0.6
0.4
0.2
0.0
$f_{\pi^0}/P(\pi^0)$
f_{π^0}
$f^l_{\pi^0} \cdot f_{\pi^0}$
0.5
1.0
5.0
10.0
50.0
100.0
500.0
E_{inc} [GeV]
64 5 1 A 6

Fig. 6

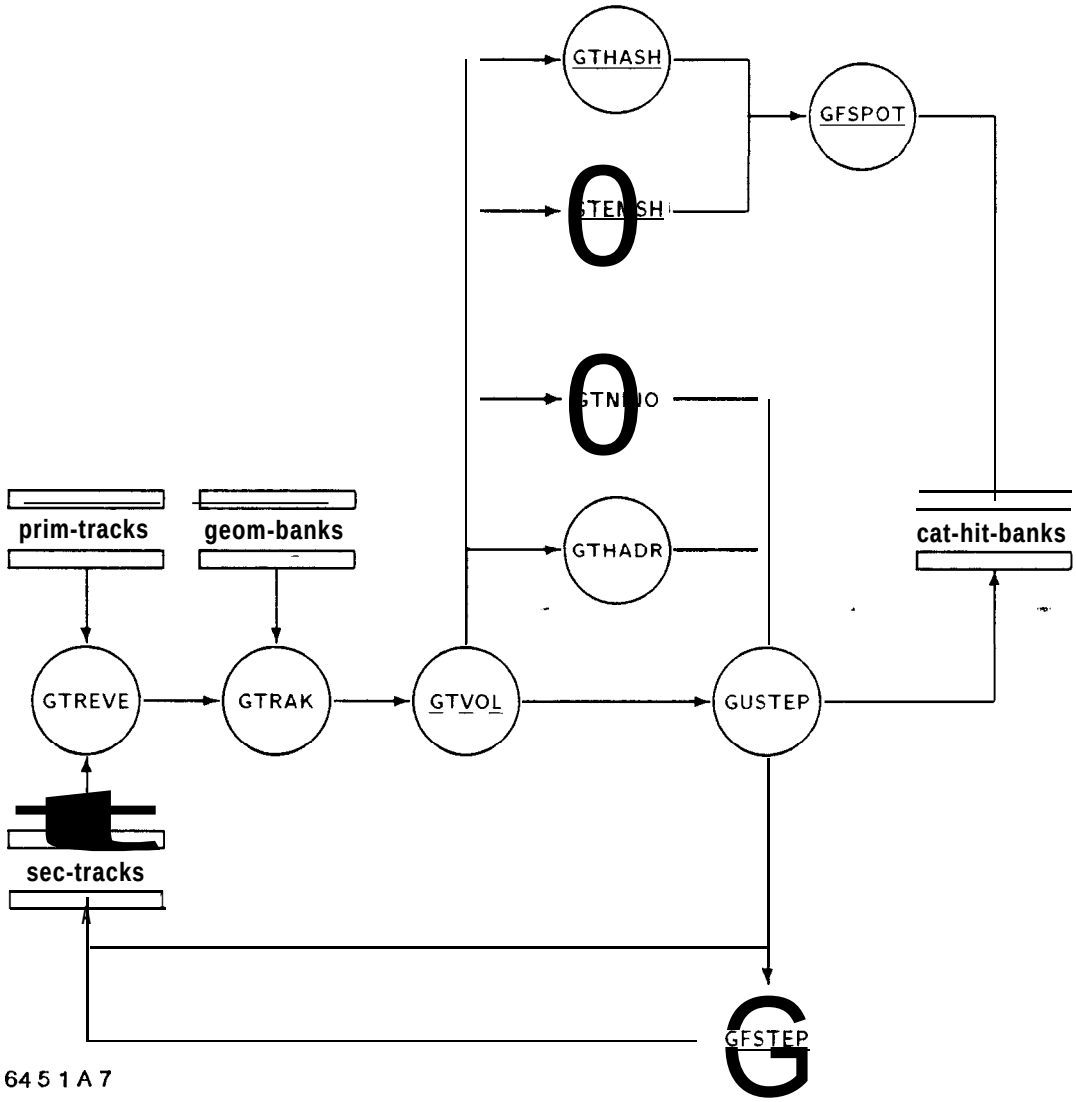
GTHASH
GFSPOT
prim-tracks
geom-banks
GTHADR
cat-hit-banks
GTREVE
GTRAK
GTVOL
GUSTEP
sec-tracks
GFSTEP
64 5 1 A 7

Fig. 7

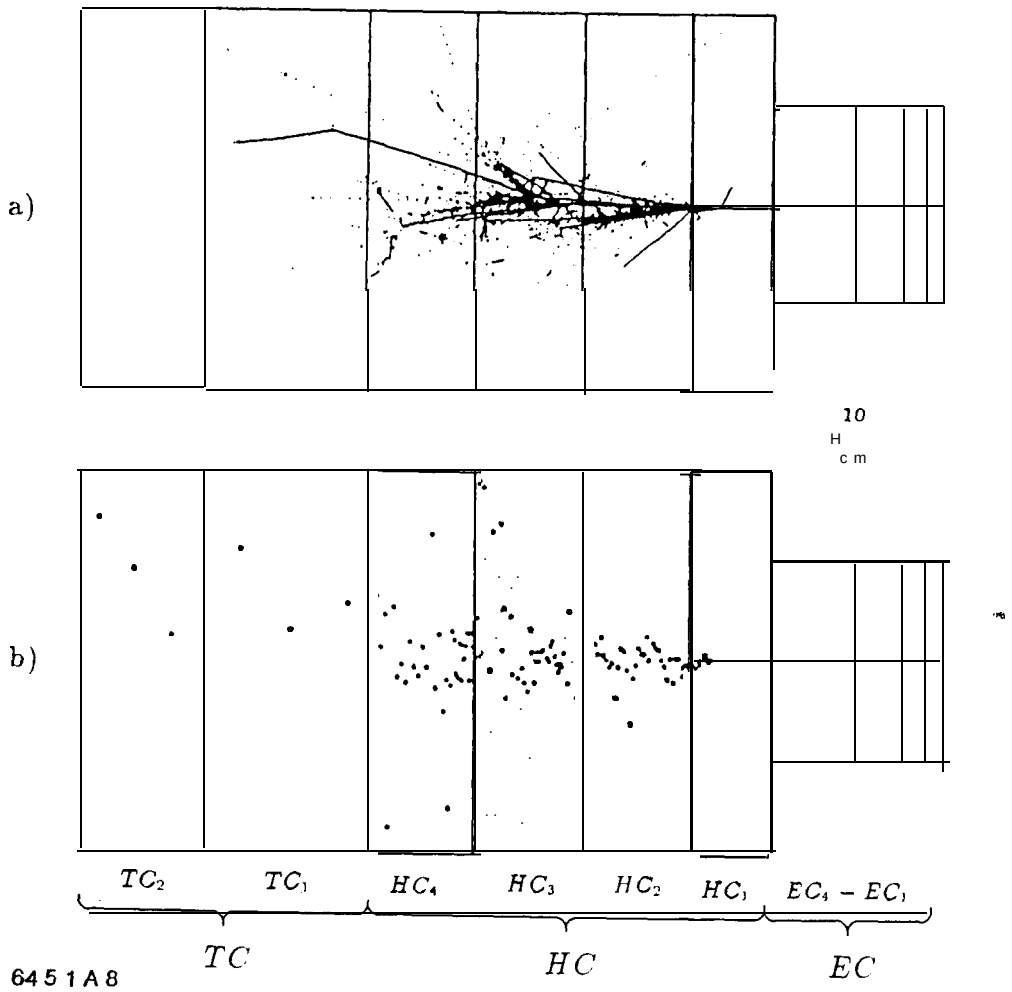

Fig. 8

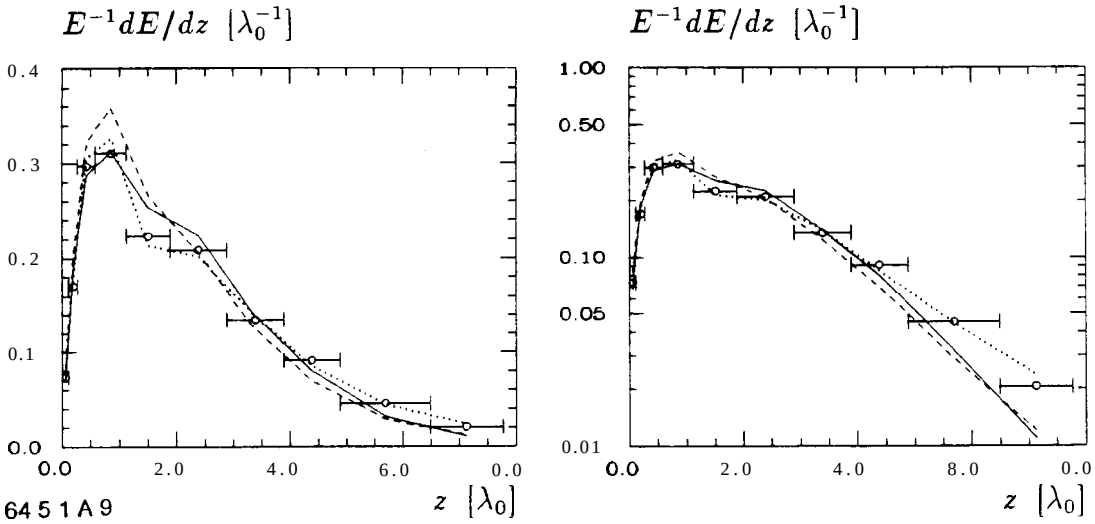
$E^{-1}dE/dz\ [\lambda_0^{-1}]$
0.4
0.3
0.2
0.1
0.0
0.0
2.0
4.0
6.0
0.0
$z\ [\lambda_0]$
64 5 1 A 9
$E^{-1}dE/dz\ [\lambda_0^{-1}]$
1.00
0.50
0.10
0.05
0.01
0.0
2.0
4.0
8.0
0.0
$z\ [\lambda_0]$

Fig. 9

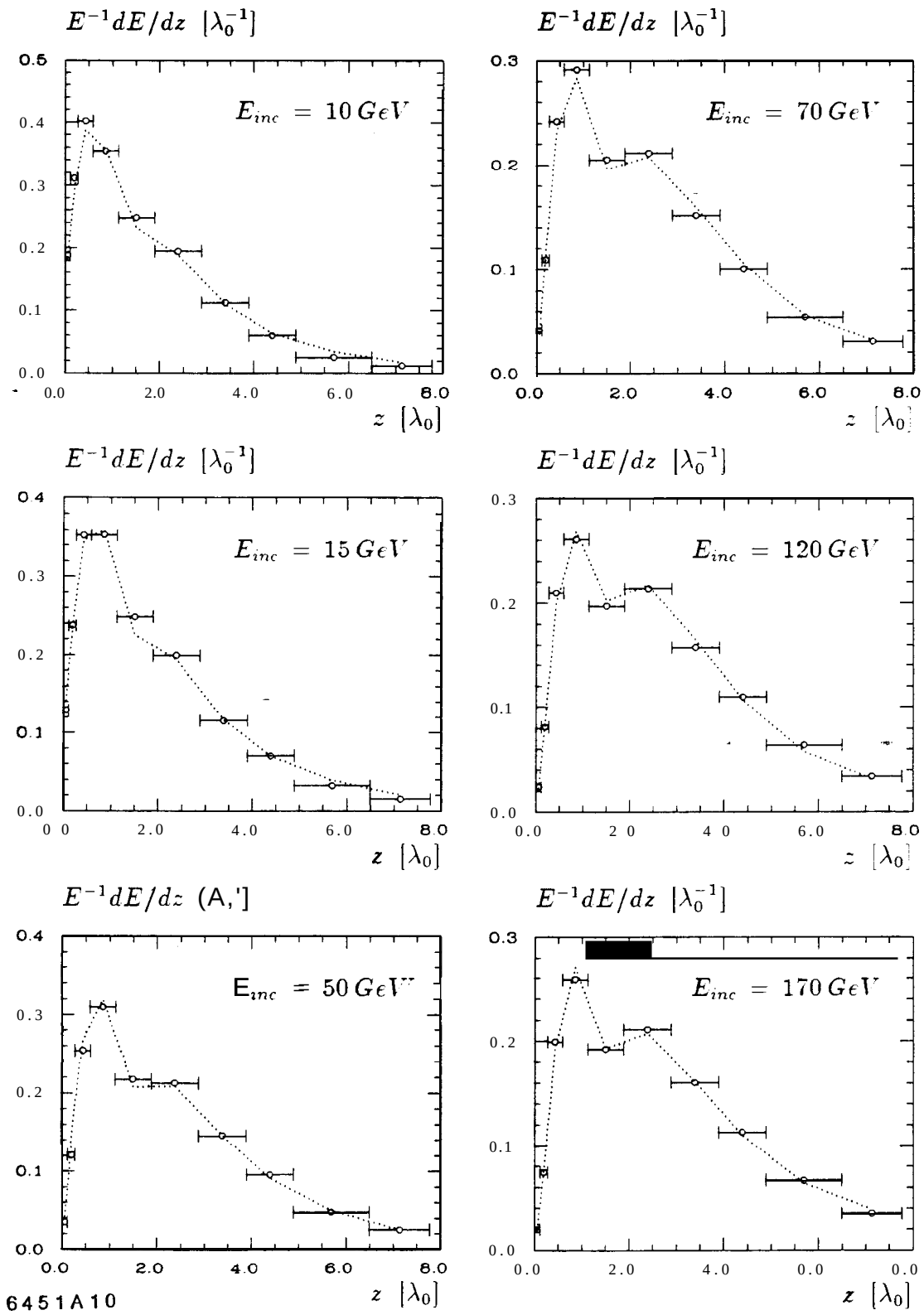
$E^{-1}dE/dz\ [\lambda_0^{-1}]$
$E_{inc} = 10\,GeV$
$z\ [\lambda_0]$
$E^{-1}dE/dz\ [\lambda_0^{-1}]$
$E_{inc} = 70\,GeV$
$z\ [\lambda_0]$
$E^{-1}dE/dz\ [\lambda_0^{-1}]$
$E_{inc} = 15\,GeV$
$z\ [\lambda_0]$
$E^{-1}dE/dz\ [\lambda_0^{-1}]$
$E_{inc} = 120\,GeV$
$z\ [\lambda_0]$
$E^{-1}dE/dz$ (A,']
$E_{inc} = 50\,GeV$
$z\ [\lambda_0]$
$E^{-1}dE/dz\ [\lambda_0^{-1}]$
$E_{inc} = 170\,GeV$
$z\ [\lambda_0]$
6451A10

Fig. 10

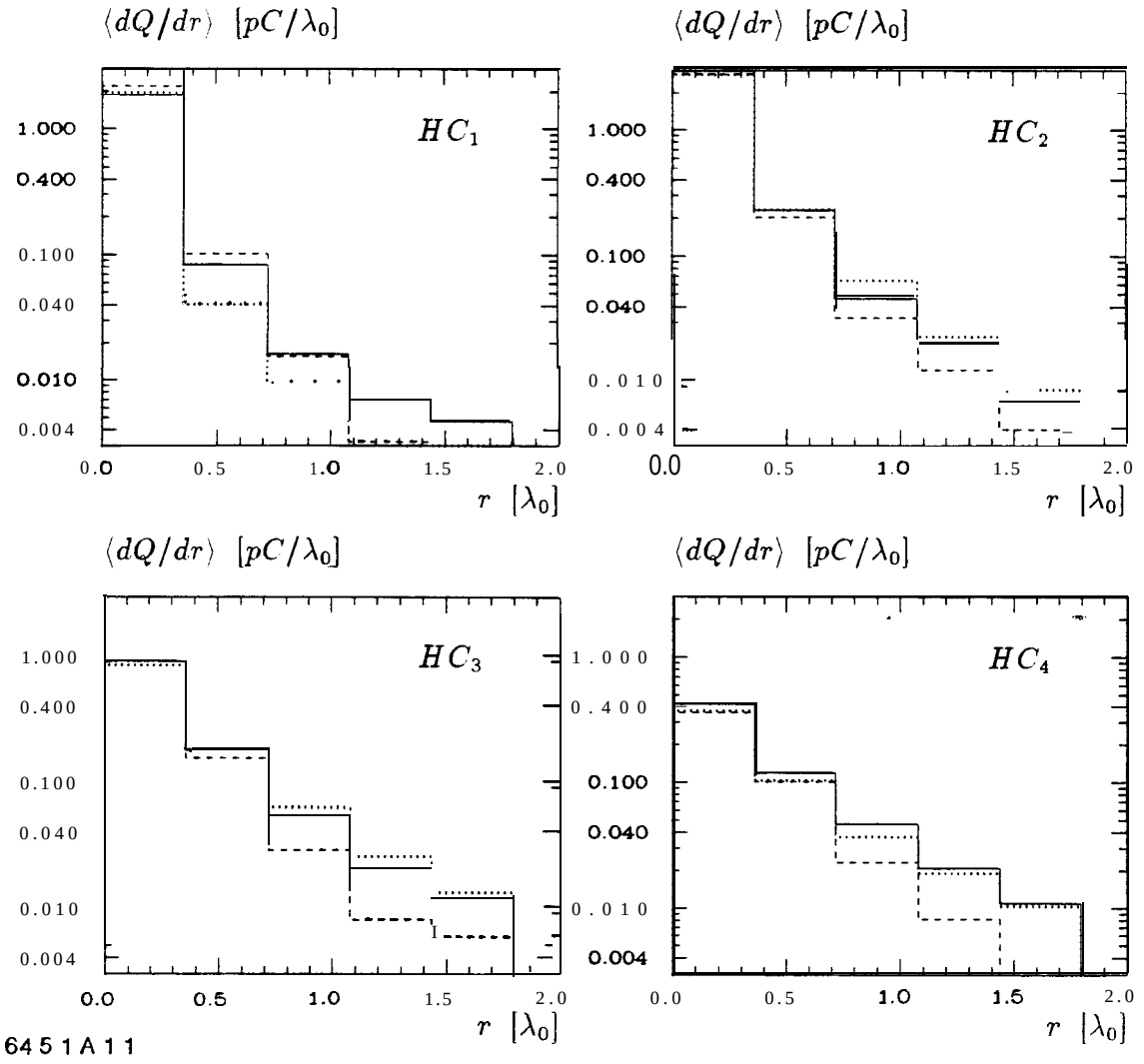
⟨dQ/dr⟩ [pC/λ0]
HC1
HC2
HC3
HC4
1.000
0.400
0.100
0.040
0.010
0.004
0.0
0.5
1.0
1.5
2.0
r [λ0]
64 5 1 A 1 1

Fig. 11

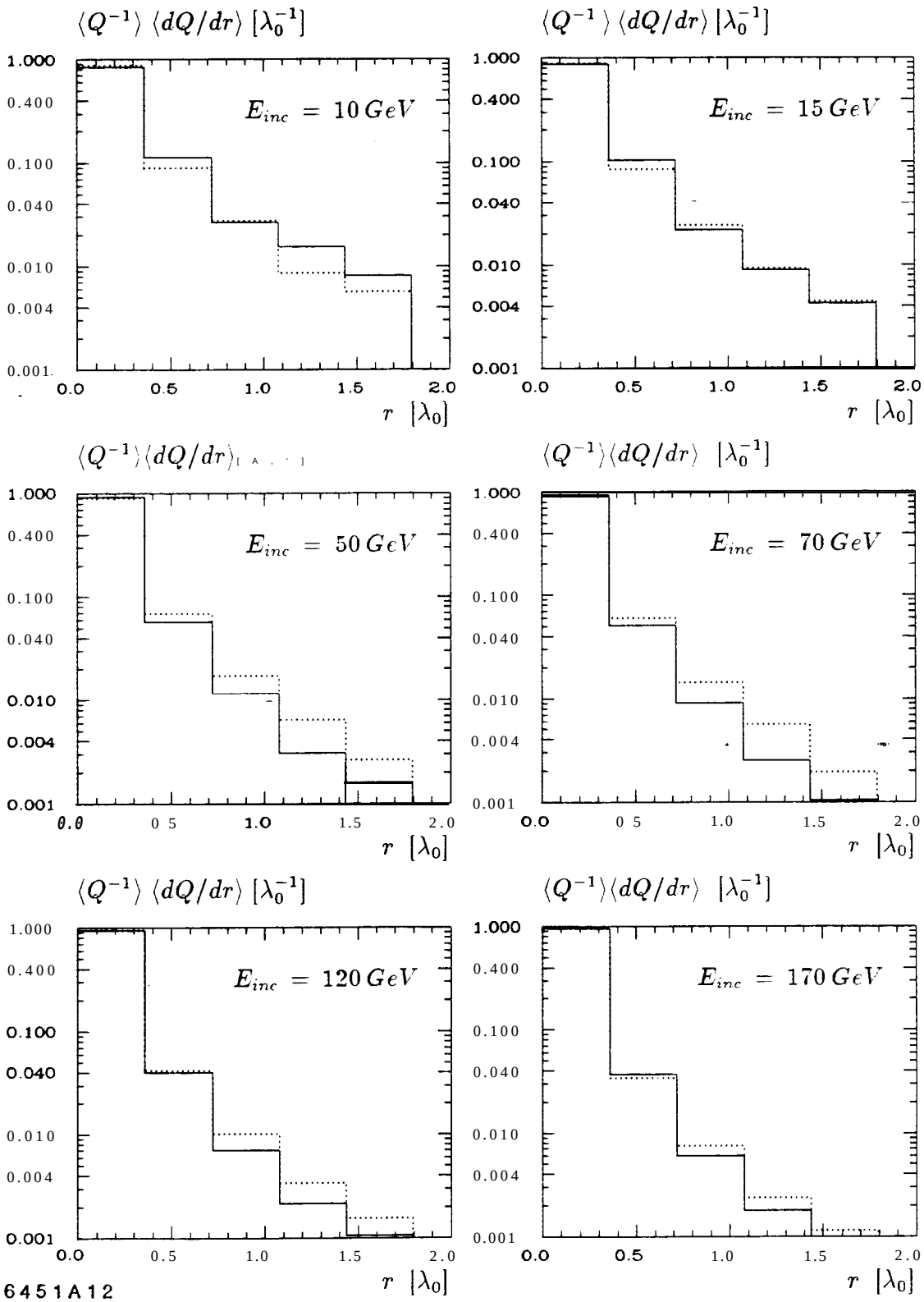
$\langle Q^{-1} \rangle \langle dQ/dr \rangle [\lambda_0^{-1}]$
$E_{inc} = 10\,GeV$
$E_{inc} = 15\,GeV$
$E_{inc} = 50\,GeV$
$E_{inc} = 70\,GeV$
$E_{inc} = 120\,GeV$
$E_{inc} = 170\,GeV$
1.000
0.400
0.100
0.040
0.010
0.004
0.001
0.0
0.5
1.0
1.5
2.0
$r\ [\lambda_0]$
6451A12

Fig. 12

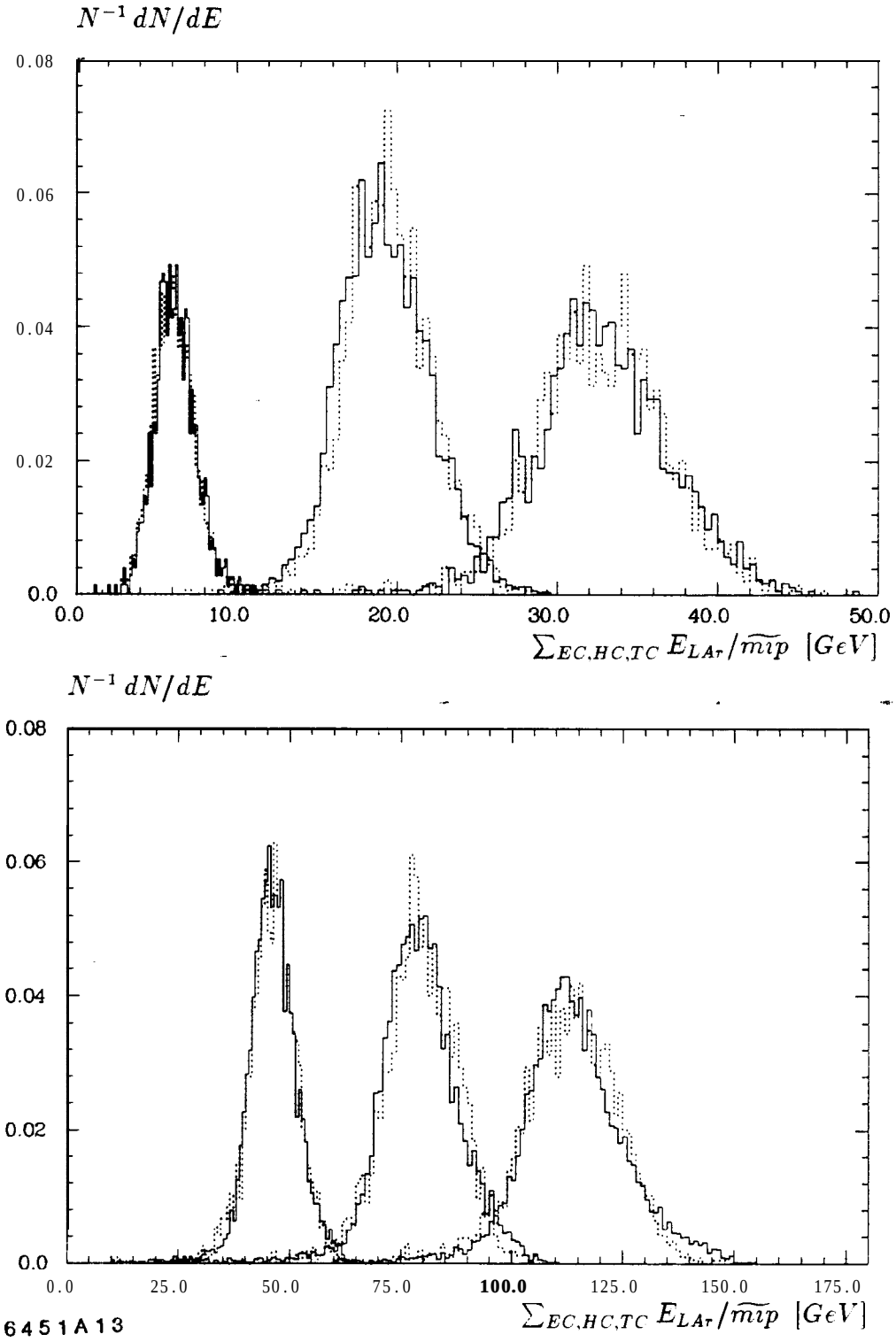
$N^{-1}\,dN/dE$
0.08
0.06
0.04
0.02
0.0
0.0
10.0
20.0
30.0
40.0
50.0
$\sum_{EC,HC,TC} E_{LAr}/\widetilde{mip}$ [GeV]
$N^{-1}\,dN/dE$
0.08
0.06
0.04
0.02
0.0
0.0
25.0
50.0
75.0
100.0
125.0
150.0
175.0
$\sum_{EC,HC,TC} E_{LAr}/\widetilde{mip}$ [GeV]
6451A13

Fig. 13

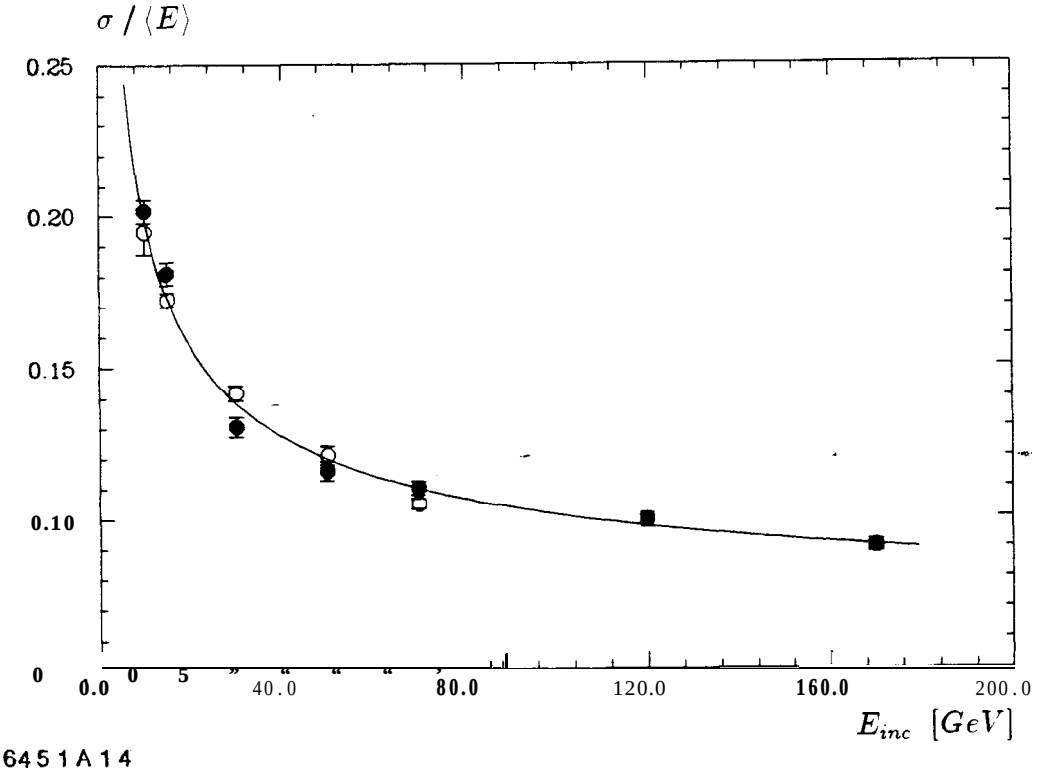

Fig. 14

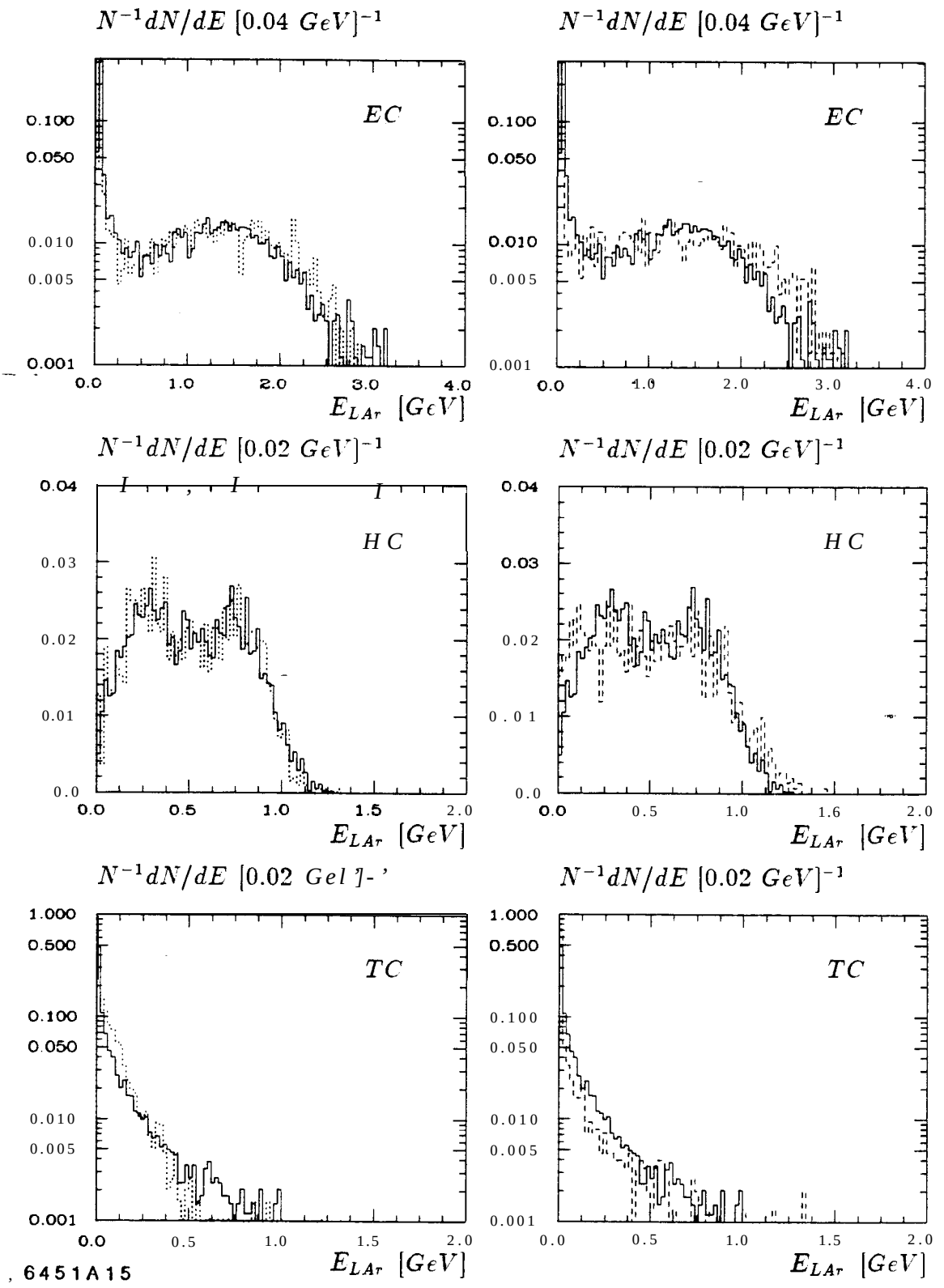
$N^{-1}dN/dE$ [0.04 GeV]$^{-1}$
EC
0.100
0.050
0.010
0.005
0.001
0.0
1.0
2.0
3.0
4.0
E_{LAr} [GeV]
$N^{-1}dN/dE$ [0.04 GeV]$^{-1}$
EC
$N^{-1}dN/dE$ [0.02 GeV]$^{-1}$
HC
0.04
0.03
0.02
0.01
0.0
0.5
1.0
1.5
2.0
E_{LAr} [GeV]
$N^{-1}dN/dE$ [0.02 GeV]$^{-1}$
HC
$N^{-1}dN/dE$ [0.02 GeV]$^{-1}$
TC
1.000
0.500
0.100
0.050
0.010
0.005
0.001
E_{LAr} [GeV]
$N^{-1}dN/dE$ [0.02 GeV]$^{-1}$
TC
6451A15

Fig. 15

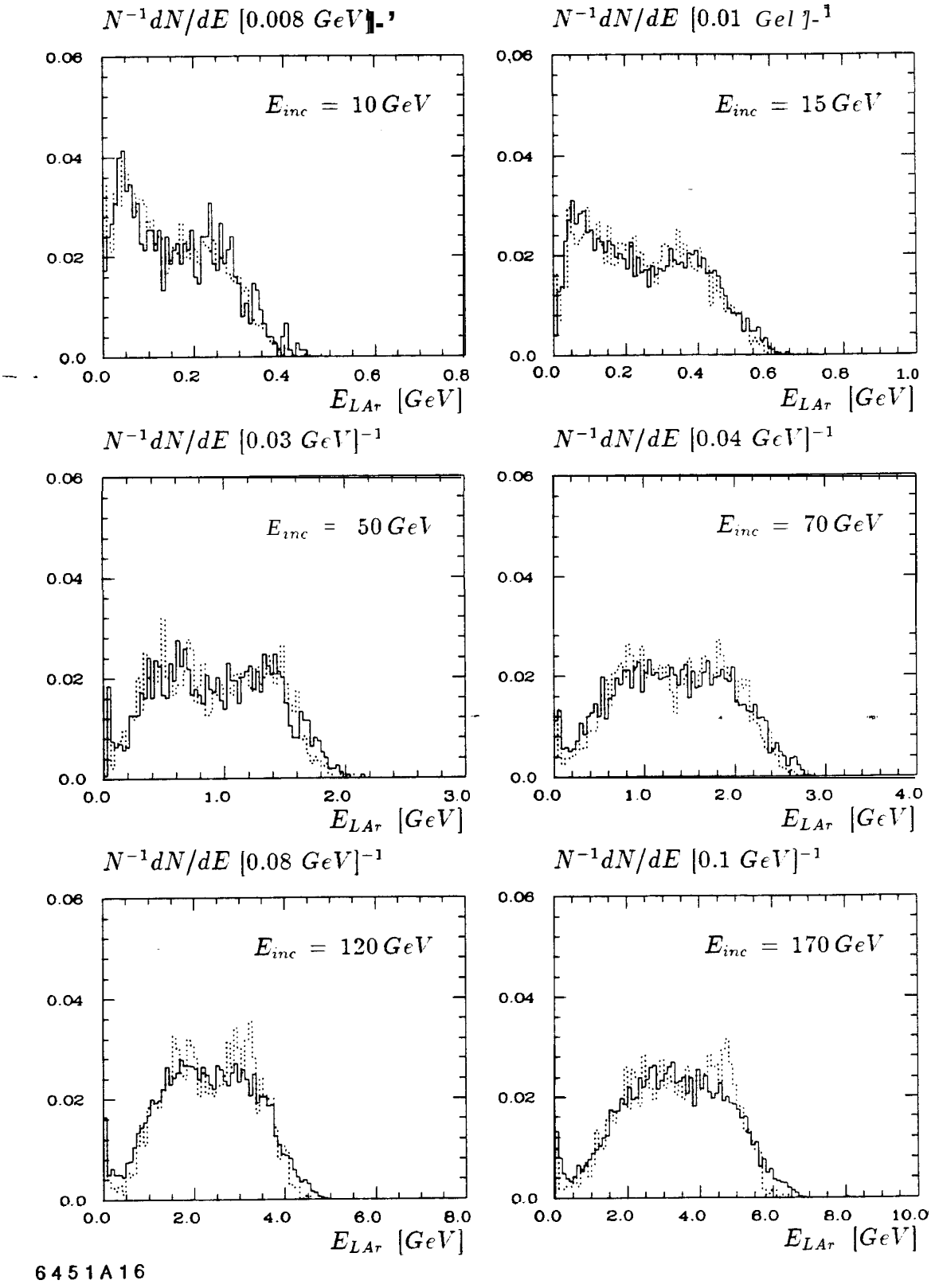
$N^{-1}dN/dE$ [0.008 GeV]$^{-1}$
E_{inc} = 10 GeV
E_{LAr} [GeV]
$N^{-1}dN/dE$ [0.01 GeV]$^{-1}$
E_{inc} = 15 GeV
E_{LAr} [GeV]
$N^{-1}dN/dE$ [0.03 GeV]$^{-1}$
E_{inc} = 50 GeV
E_{LAr} [GeV]
$N^{-1}dN/dE$ [0.04 GeV]$^{-1}$
E_{inc} = 70 GeV
E_{LAr} [GeV]
$N^{-1}dN/dE$ [0.08 GeV]$^{-1}$
E_{inc} = 120 GeV
E_{LAr} [GeV]
$N^{-1}dN/dE$ [0.1 GeV]$^{-1}$
E_{inc} = 170 GeV
E_{LAr} [GeV]
6451A16

Fig. 16

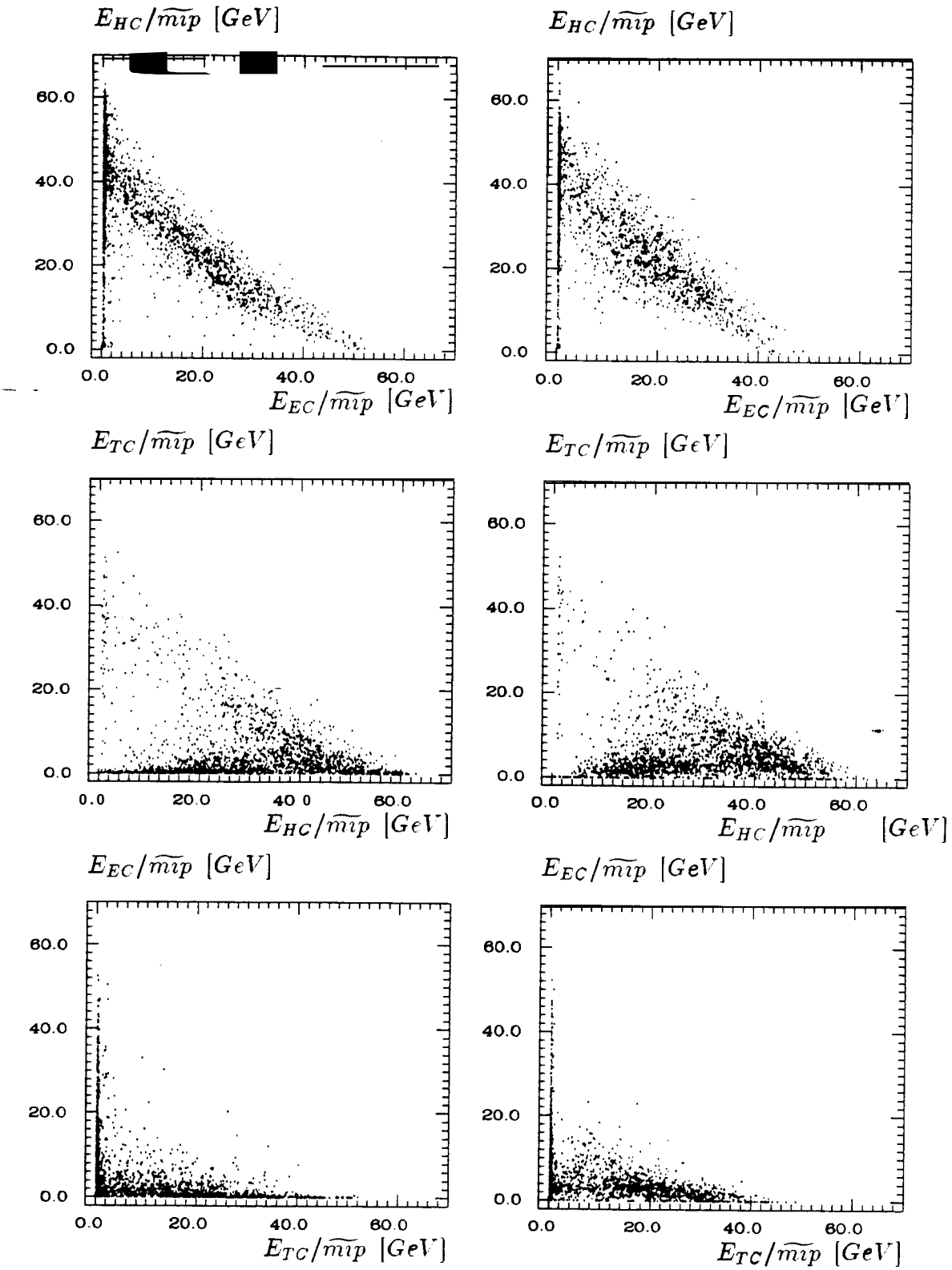
$E_{HC}/\widetilde{mip}$ [GeV]
$E_{EC}/\widetilde{mip}$ [GeV]
$E_{HC}/\widetilde{mip}$ [GeV]
$E_{EC}/\widetilde{mip}$ [GeV]
$E_{TC}/\widetilde{mip}$ [GeV]
$E_{HC}/\widetilde{mip}$ [GeV]
$E_{TC}/\widetilde{mip}$ [GeV]
$E_{HC}/\widetilde{mip}$ [GeV]
$E_{EC}/\widetilde{mip}$ [GeV]
$E_{TC}/\widetilde{mip}$ [GeV]
$E_{EC}/\widetilde{mip}$ [GeV]
$E_{TC}/\widetilde{mip}$ [GeV]
0.0
20.0
40.0
60.0
6451A17

Fig. 17